Low-dissipation edge currents without edge states

Justin C. W. Song[1,2,*] and Giovanni Vignale[3,4,5]

[1]*Division of Physics and Applied Physics, Nanyang Technological University, 637371 Singapore, Singapore*
[2]*Institute of High Performance Computing, Agency for Science, Technology, and Research, 138632 Singapore, Singapore*
[3]*Department of Physics and Astronomy, University of Missouri, Columbia, Missouri 65211, USA*
[4]*Center for Advanced 2D Materials, National University of Singapore, 117542 Singapore, Singapore*
[5]*Yale-NUS College, 16 College Avenue West, 138527 Singapore, Singapore*

(Received 28 May 2018; revised manuscript received 18 October 2018; published 6 June 2019)

We propose that bulk free carriers in topologically trivial multivalley insulators with nonvanishing Berry curvature can give rise to low-dissipation edge currents, which are squeezed within a distance on the order of the valley diffusion length from the edge. This happens even in the absence of edge states [topological (gapless) or otherwise], and when the bulk equilibrium carrier concentration is thermally activated across the gap. Physically, the squeezed edge current arises from the spatially inhomogeneous valley orbital magnetization that develops from valley-density accumulation near the edge. While this current possesses neither topology nor symmetry protection and, as a result, is not immune to dissipation, in clean enough devices it can mimic low-loss ballistic transport.

DOI: 10.1103/PhysRevB.99.235405

I. INTRODUCTION

In bulk band insulators, carrier transport is exponentially activated, leading to a severely muted current response when an electric field is applied [1]. However, this adage fails spectacularly in topological matter where gapped bulk bands, characterized by a nontrivial topology [2,3], support gapless edge states [3–6], which can carry dissipationless charge currents along the edges of the sample. As a result, such edge currents have become synonymous with topologically nontrivial bulk bands as expected from the principle of bulk-edge correspondence [3,6–8].

Here we argue that in the presence of Bloch-band Berry curvature, bulk free carriers in a multivalley gapped insulator can conspire to produce a charge current that is squeezed close to sample boundaries in the absence of edge states (Fig. 1). The squeezed edge current (SEC) [Fig. 1(b)] has low (but finite) dissipation and occurs even when the equilibrium chemical potential is in the gap with a thermally activated bulk. As a result, SEC can act as a current conduit shunting the nominally insulating bulk to produce unusual nonactivated resistivity characteristics at low temperature.

We expect SEC to naturally manifest in topologically trivial insulators possessing well-separated Bloch-band Berry curvature distributions [9] in the Brillouin zone (e.g., in Fig. 1), such that the total integrated curvature is zero. These systems do not possess gapless topologically protected edge states. Instead, the Berry curvature in each of the valleys enables valley Hall currents to be induced by an applied electric field and produce a valley density accumulation (of bulk carriers) near the edge of the sample, while the net charge density remains zero. The valley density gradient perpendicular to the edge produces a charge current flowing along the edge. This induced charge current (transverse to the valley density gradient) can be viewed as an anomalous transverse diffusion of carriers, with off-diagonal diffusion constants of different signs in different valleys—a characteristic of carriers possessing finite Berry curvature.

SEC appears only in finite-sized samples (e.g., Hall-bar type geometries) and vanishes in the infinite bulk or when measurements exclude edge currents (e.g., Corbino geometries); see Fig. 2. While located close to sample boundaries, we emphasize that SEC arises from bulk carriers; it occurs in the absence of localized edge modes of either topological (gapless) edge state origin or from other sources (e.g., band bending [10,11], gapped edge modes on rough boundaries [12]). Instead, SEC is intimately tied to a current-induced bulk and out-of-local-equilibrium magnetization buildup (pointing out-of-plane) at sample edges that has been recently measured in gapped Dirac systems [13,14]. The resulting out-of-local-equilibrium (magnetoelectric) currents are the origin of the nonactivated transport characteristics we unveil below.

While gapped graphene-type systems are not the only examples of this type of behavior, they present natural experimental targets due to their high quality, ease of manipulation, lack of topological gapless edge states, and clear observations of bulk valley Hall currents [15–17]. Indeed, a recent experiment that infers edge-type currents in topologically trivial systems [18] provides strong indications of SEC in gapped Dirac systems; see discussion below.

II. INHOMOGENEOUS VALLEY HALL CURRENTS

We begin by recalling that the position and velocity operators within a Bloch band (l) and valley (α) are

$$\hat{\mathbf{r}}_{l\alpha} = i\frac{\partial}{\partial \mathbf{k}} + \boldsymbol{\mathcal{A}}_{l\alpha}(\mathbf{k}), \quad \hat{\mathbf{v}}_{l\alpha} = \frac{1}{i\hbar}[\hat{\mathbf{r}}_{l\alpha}, \hat{H}], \tag{1}$$

*justinsong@ntu.edu.sg

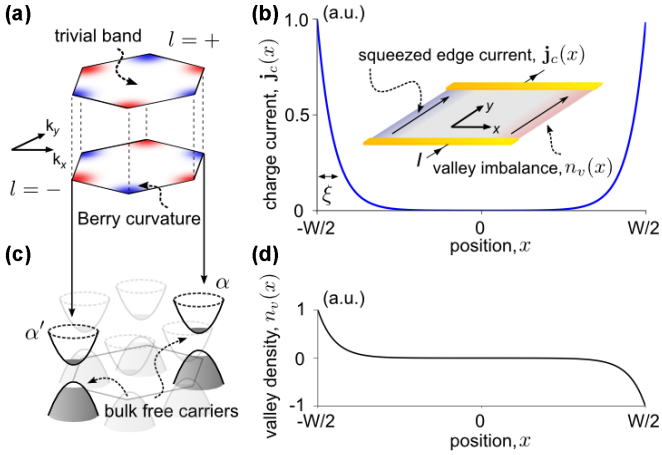

FIG. 1. Squeezed edge currents in a topologically trivial insulator. (a) Berry curvature hot spots in topologically trivial insulator bands with zero net Berry flux over the entire Brillouin zone, e.g., (shown) Berry curvature, $\Omega_{l\alpha}$ hot spots for gapped graphene with broken inversion symmetry; $l = \pm$ are conduction and valence bands. (b) A *charged* squeezed edge current (SEC), $\mathbf{j}_c(\mathbf{r})$, can flow along the sample edges [Eq. (9)] even in a gapped finite-sized device (inset) without edge states. (c) Carriers in highlighted bands at α, α' experience opposite signs of Berry curvature and contrasting transport characteristics (see text). (d) Density imbalance between flavors/valleys can accumulate at sample edges over a width determined by the flavor/valley diffusion length ξ, Eq. (7). We have used $\Omega_{l\alpha}$ for a gapped Dirac material (see text) so that $\sigma_H^v > 0$ and $D_H^v < 0$ [Eqs. (4) and (5)].

where $\mathcal{A}_{l\alpha}(\mathbf{k}) = i\langle u_{l\alpha}(\mathbf{k})|\nabla_{\mathbf{k}} u_{l\alpha}(\mathbf{k})\rangle$ is the Berry connection of the band and valley under consideration. We note that the band velocity reproduces the familiar $\langle u_{l\alpha}(\mathbf{k})|\hat{\mathbf{v}}_{l\alpha}|u_{l\alpha}(\mathbf{k})\rangle = \frac{d\epsilon_{l\alpha}(\mathbf{k})}{\hbar\partial\mathbf{k}} - \hbar^{-1}e\boldsymbol{\Omega}_{l\alpha}(\mathbf{k}) \times \mathbf{E}$, where $\boldsymbol{\Omega}_{l\alpha}(\mathbf{k}) = \nabla_{\mathbf{k}} \times \mathcal{A}_{l\alpha}(\mathbf{k})$ is the Berry curvature, $\epsilon_{l\alpha}$ is the band energy, and $-e<0$ is the electron charge. The Berry curvature is of order λ^2, where λ plays the role of an effective "Compton wavelength," inversely proportional to the gap at the band extrema (an explicit expression for "gapped graphene" will be given later). The above expressions are invariant under a gauge transformation that multiplies the Bloch wave function by a $\mathbf{k}$-dependent phase.

We now construct the current density fluctuation operator at wave vector $\mathbf{q}$ (for a single particle) as follows: $\hat{\mathbf{j}}_{l\alpha}(\mathbf{q}) = -\frac{e}{2}(\hat{\mathbf{v}}_{l\alpha}e^{-i\mathbf{q}\cdot\hat{\mathbf{r}}_{l\alpha}} + e^{-i\mathbf{q}\cdot\hat{\mathbf{r}}_{l\alpha}}\hat{\mathbf{v}}_{l\alpha})$. We will be interested in current distributions that are slowly varying on the scale of λ. In this regime, we can expand $\hat{\mathbf{j}}_{l\alpha}(\mathbf{q})$ to first order in $\mathbf{q}$:

$$\hat{\mathbf{j}}_{l\alpha}(\mathbf{q}) = -e\hat{\mathbf{v}}_{l\alpha} + \frac{i}{2}e[(\mathbf{q}\cdot\hat{\mathbf{r}}_{l\alpha})\hat{\mathbf{v}}_{l\alpha} + \hat{\mathbf{v}}_{l\alpha}(\mathbf{q}\cdot\hat{\mathbf{r}}_{l\alpha})]. \quad (2)$$

While the first term in Eq. (2) is the homogeneous current ($\mathbf{q} = 0$), see Eq. (1), the second term only becomes relevant in an inhomogeneous system. Taking the latter's expectation value for state $|u_{l\alpha}(\mathbf{k})\rangle$ yields a purely transverse current $i\mathbf{q} \times \mathbf{m}_{l\alpha}(\mathbf{k})$, where $\mathbf{m}_{l\alpha}(\mathbf{k}) = -\frac{e}{4}(\hat{\mathbf{r}} \times \hat{\mathbf{v}} - \hat{\mathbf{v}} \times \hat{\mathbf{r}})$ is the magnetic moment [19]; see Appendix B.

The full physical current density in real space $\mathbf{j}_{l\alpha}(\mathbf{r})$ proceeds directly from Eq. (2). Performing an inverse Fourier transformation and averaging over a nonequilibrium state described by the inhomogeneous electron distribution function $f_{l\alpha}(\mathbf{k}, \mathbf{r})$ yields

$$\mathbf{j}_{l\alpha}(\mathbf{r}) = \sum_{\mathbf{k}} \left[-e\frac{\partial\epsilon_{l\alpha}(\mathbf{k})}{\hbar\partial\mathbf{k}} + \frac{e\boldsymbol{\Omega}_{l\alpha}(\mathbf{k})}{\hbar} \times e\mathbf{E} \right] f_{l\alpha}(\mathbf{k}, \mathbf{r}) + \sum_{\mathbf{k}} \frac{\partial f_{l\alpha}(\mathbf{k}, \mathbf{r})}{\partial\mathbf{r}} \times \mathbf{m}_{l\alpha}(\mathbf{k}). \quad (3)$$

The first term of Eq. (3) is the familiar homogeneous current (including a homogeneous Hall current driven by an electric field) [20]. The second term is the current driven by an electron density gradient and exists even in the absence of direct mechanical forces, such as an applied electric field [21,22]. The latter is the *Hall diffusion current,* which must necessarily accompany electric-field-driven Hall currents whenever the density is nonuniform.

We emphasize that Eq. (3) is the full physical current that can be measured using local probes (e.g., via scanning nitrogen vacancy center microscopy [23]). Even so, we note that in transport experiments, the charge current collected by leads attached to device boundaries is sensitive to the *net* charge current moving through the cross section of the device. For example, charge transport is insensitive to circulating currents that may occur deep in the bulk, as illustrated in Ref. [24] by integrating through a device cross section.

As a result, to ensure that we capture the transport of charge we explicitly take a cross section over the entire sample and integrate the net current flowing through it; see below. As we will see, this leads to SEC freely flowing in the same direction along the edges (Fig. 1), being fed by external contacts.

III. SQUEEZED EDGE CURRENTS

In order to illustrate SEC, we focus on a prototypical nontopological insulator: a gapped Dirac material where inversion symmetry is broken (e.g., gapped graphene on hexagonal boron nitride) with a Hamiltonian around each of the valleys as $\mathcal{H}_\alpha = v\hbar(k_x\tau_x + \alpha k_y\tau_y) + \Delta\tau_z$ (where $\tau_{x,y,z}$ are Pauli matrices) and $\alpha = \pm 1$ for K, K' valleys, respectively; see Fig. 1. The Berry curvature is concentrated in hot spots close to the two inequivalent valleys $\alpha = \{K, K'\}$ and is given by $\boldsymbol{\Omega}_{l\alpha}(\mathbf{k}) = -\frac{\alpha\lambda^2}{2}\frac{\Delta^3}{\epsilon_l^3(\mathbf{k})}\hat{\mathbf{z}}$, where $\lambda = \frac{\hbar v}{\Delta}$. The magnetic moment is given by $\mathbf{m}_{\ell\alpha}(\mathbf{k}) = \frac{e}{\hbar}\epsilon_{\mathbf{k},\ell}\boldsymbol{\Omega}_{\ell\alpha}(\mathbf{k})$ (see Appendix C). For brevity, we will drop the vector notation for Berry curvature since $\boldsymbol{\Omega}(\mathbf{k}) = \Omega(\mathbf{k})\hat{\mathbf{z}}$ in two-dimensional systems. Total *charge current* (c) is determined by $\mathbf{j}_c \equiv \sum_{l,\alpha}\mathbf{j}_{l,\alpha}$ and the total *valley current* (v) is $\mathbf{j}_v \equiv \sum_{l\alpha}\alpha\mathbf{j}_{l,\alpha}$, where $\alpha = 1$ for K and $\alpha = -1$ for K'. Similarly, we write charge and valley densities as $n_c \equiv \sum_{l,\alpha} n_{l\alpha}$ and $n_v \equiv \sum_{l,\alpha}\alpha n_{l\alpha}$; here $n_{l\alpha}(\mathbf{r}) = \sum_{\mathbf{k}}(-e)f_{l\alpha}(\mathbf{k}, \mathbf{r})$ is the charge density in l, α.

Since $\Omega_{l\alpha}(\mathbf{k})$ changes sign in going from $\alpha = K$ to $\alpha = K'$, the flow of charge currents is particularly sensitive to the imbalance of distribution function between valleys. To see this, using Eq. (3), we construct the total charge and valley currents in each band l explicitly as

$$\begin{aligned} \mathbf{j}_c &= -D\nabla n_c + \sigma\mathbf{E} - D_H^v[(\nabla n_v) \times \hat{\mathbf{z}}], \\ \mathbf{j}_v &= -D\nabla n_v + \left[\sigma_H^v\right]\hat{\mathbf{z}} \times \mathbf{E} - D_H^v[(\nabla n_c) \times \hat{\mathbf{z}}], \end{aligned} \quad (4)$$

where D is the ordinary *longitudinal* diffusion constant of carriers within the bands, σ is the longitudinal conductivity, and $[\sigma_H^v] = (e^2/\hbar)\sum_{\mathbf{k},l,\alpha} \alpha\Omega_{l\alpha} f_{l\alpha}^{(0)}(\mathbf{k})$ is the valley Hall conductivity; $f_{l\alpha}^{(0)}(\mathbf{k})$ is the Fermi-Dirac function $f_{l\alpha}^{(0)}(\mathbf{k}) = (1 + \exp\{[\epsilon_l(\mathbf{k}) - \mu_{l\alpha}]/(k_BT)\})^{-1}$ with $\mu_{l\alpha}$ the (quasi)chemical potential. Crucially, D_H^v is the *valley Hall diffusion constant*, which captures the transverse current flow arising from an inhomogeneous distribution function in each of the valleys: $\mathbf{j}_{l\alpha} = -D_H^{l\alpha}\nabla n_{l\alpha} \times \hat{\mathbf{z}}$, where for gapped graphene we have

$$D_H^{l\alpha} = \frac{\sum_{\mathbf{k}} \epsilon_l(\mathbf{k})\Omega_{l\alpha}(\mathbf{k})\frac{\partial f_{l\alpha}^{(0)}(\mathbf{k})}{\partial \mu_{l\alpha}}}{\hbar \sum_{\mathbf{k}} \frac{\partial f_{l\alpha}^{(0)}(\mathbf{k})}{\partial \mu_{l\alpha}}}. \tag{5}$$

Since $\Omega_{l\alpha}(\mathbf{k})$ changes sign when either the band index or the valley index is switched, $D^{+,\alpha} = D_H^{-,\alpha} = \alpha D_H^v$, where $D_H^v \equiv D_H^{l=+,\alpha=+1}$. Summing $\mathbf{j}_{l\alpha}$ over l and α gives the inhomogeneous charge current as written in Eq. (4).

When an electric field is applied along the sample, the bulk valley Hall effect produces a valley Hall current that must be canceled by a valley density gradient perpendicular to the sample boundaries. This dramatically impacts *charge* transport characteristics. The profiles of density imbalance between valleys in each band $n_v(\mathbf{r})$ obey the diffusion equation

$$\partial_t n_v(\mathbf{r}) - D\nabla^2 n_v(\mathbf{r}) + \frac{n_v(\mathbf{r})}{\tau_v} = -\nabla \cdot \left([\sigma_H^v]\hat{\mathbf{z}} \times \mathbf{E}\right), \tag{6}$$

where τ_v is the intervalley scattering time between valleys that captures the rate at which disparate parts (at K and K') of the Fermi surface equilibrate with each other. In the nondegenerate limit, the longitudinal diffusion can be estimated as $D = k_BT\eta/e$, where η is the mobility; here we have used the same diffusion constant in both conduction and valence bands for simplicity. Different diffusion constants can be implemented with no qualitative change to the results below.

Considering a long Hall bar, $L \gg W$, we treat $n_v(\mathbf{r})$ and $\mathbf{E}(\mathbf{r})$ as independent of y along the bar; this reduces Eq. (6), in the steady state, to a one-dimensional differential equation, with the density jumping from a finite value to zero at $x = \pm W/2$. Further, by focusing on regions far away from contacts, we treat the electric field as uniform. As a result, $n_v(\mathbf{r})$ is driven only by delta-function sources at the boundaries $x = \pm W/2$: $-\nabla \cdot ([\sigma_H^v]\hat{\mathbf{z}} \times \mathbf{E}) = -[\sigma_H^v]E[\delta(x - W/2) - \delta(x + W/2)]$, where $\mathbf{E} = E\hat{\mathbf{y}}$. We note that σ_H^v is maximal when the chemical potential is in the gap [25].

The solution of the differential equation is found by elementary means to be

$$n_v(x) = -\frac{[\sigma_H^v]E\tau_v}{\xi \cosh(W/2\xi)} \sinh\left(\frac{x}{\xi}\right) \tag{7}$$

for $|x| \leqslant W/2$, and 0 otherwise. Here $\xi = \sqrt{D\tau_v}$ is the valley diffusion length. As shown in Fig. 1(d), valley density accumulates at the edges.

We emphasize that our diffusive treatment is valid only when the spatial profile of n_v, $\mathbf{j}_c$ is slowly varying on the scale of the Compton wavelength $\lambda = \hbar v/\Delta$, the typical length scale of the wave packets close to the band edge in a gapped Dirac model. $\lambda \simeq 6 \times 10^{-8}$ m for $v = 10^6$ m s^{-1} and half-gap size $\Delta = 10$ meV. The typical scale of $n_v(\mathbf{r})$ variation is captured by the diffusion length ξ. As a result, we expect that our semiclassical diffusive picture holds as long as $\xi \gg \lambda$. Using the nondegenerate form of longitudinal diffusion constant $D = k_BT\eta/e$ we find that this occurs for large enough temperatures

$$T \gg T_0, \quad k_BT_0 = \frac{e\lambda^2}{\eta\tau_v}. \tag{8}$$

Using a mobility $\eta = 1$ m^2/(V s), $\tau_v = 10$ ps we estimate $k_BT_0 \approx 0.4$ meV ($T_0 \approx 5$ K). Below this temperature scale (set by T_0), a fully quantum mechanical treatment is needed, which is beyond the scope of the present work. In spite of this, the temperature regime $\Delta > T > T_0$ (in which our treatment is valid) defines a large and technologically important temperature regime.

Applying the inhomogeneous valley density profile in Eq. (7) to Eq. (4) yields a charge current density flowing along the edge (see Fig. 1) as

$$\mathbf{j}_c^{\mathrm{SEC}}(\mathbf{r}) = j_c^{\mathrm{SEC}}(\mathbf{r})\hat{\mathbf{y}}, \quad j_c^{\mathrm{SEC}}(\mathbf{r}) = D_H^v \partial_x n_v(\mathbf{r}). \tag{9}$$

In the limit $\xi \ll W$, $\mathbf{j}_c^{\mathrm{SEC}}(\mathbf{r})$ form squeezed quasi-one-dimensional channels flowing along the edges of the Hall bar. Crucially, Eq. (9) yields two squeezed current channels flowing in the *same* direction as shown in Fig. 1; $\mathbf{j}_c^{\mathrm{SEC}}(\mathbf{r})$ flows along $\mathbf{E}$. This demonstrates that the diffusion current arising from the inhomogeneous electron distribution [see Eq. (3)] is not circulating, but contributes to total charge transport in the device.

Integrating the current density over one of these SEC channels and writing $E = V/L$, where V is the voltage drop over length L, yields $I_{\mathrm{SEC}} = \int_0^{W/2} j_c^{\mathrm{SEC}}(x)dx = -D_H^v\sigma_H^v\tau_v V/(\xi L)$. I_{SEC} constitutes a distinctly new parallel channel for current to flow in the Hall bar. We note that $-D_H^v\sigma_H^v$ is positive; see Fig. 1. Adding the current flowing in the bulk, as well as accounting for contact resistance, we find the device resistance

$$R^{-1} = R_{\mathrm{bulk}}^{-1} + R_{\mathrm{SEC}}^{-1}, \; R_{\mathrm{SEC}} = (\rho_{1\mathrm{d}}L) + R_{\mathrm{contact}}, \tag{10}$$

where $\rho_{1\mathrm{d}} = \xi/(|D_H^v\sigma_H^v|\tau_v)$, and R_{bulk} is the resistance of the bulk. Crucially, D_H^v, σ_H^v arise from the Berry curvature of the bands and exhibit a nonactivated behavior in temperature, even when the chemical potential is in the gap. As we will see, this yields $\rho_{1\mathrm{d}}$ that does not exponentially rise at low temperatures in stark contrast with R_{bulk} that exponentially rises at low temperatures.

IV. LOW-DISSIPATION SEC CHANNELS

In the nondegenerate limit $\mu_{l\alpha}, k_BT \ll \Delta$, we estimate $\sigma_H^v \approx 2e^2/h$ for an almost fully filled band (accounting for spin degeneracy). Similarly, D_H^v can be estimated from Eq. (5) in the same limit as

$$D_H^{l\alpha} \approx \alpha\frac{\hbar v^2}{2\Delta}\mathcal{F}(\tilde{\beta}), \quad \mathcal{F}(\tilde{\beta}) = \frac{-\tilde{\beta}^2\mathrm{Ei}(-\tilde{\beta})}{(1+\tilde{\beta})\exp(-\tilde{\beta})}, \tag{11}$$

where $\tilde{\beta} = \Delta/k_BT$, $\mathrm{Ei}(x) = -\int_{-x}^{\infty} dte^{-t}/t$ is the exponential integral, and we have approximated $(1 + \exp[\tilde{\beta}])^{-1} \approx$

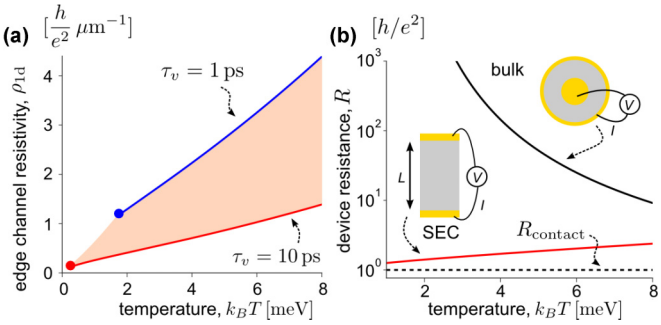

FIG. 2. Low-dissipation squeezed edge channels. (a) One-dimensional resistivity of a single squeezed edge current (SEC) channel along the edge of gapped graphene device [Eq. (12)] shown for $\tau_v = 10$ ps (red dashed) and $\tau_v = 1$ ps (blue dashed). τ_v in between these two values occupy the shaded orange region. Red and blue dots indicate temperature T_0 above which the semiclassical treatment is valid for the respective τ_v [see Eq. (8)]. (b) Device resistance for a Hall-bar device (red, $L = 1$ μm and $\tau_v = 10$ ps) and a Corbino device (black). For illustration we used parameters $\Delta = 15$ meV, $\eta = 2$ m^2/(V s), and $\sigma_H^v = 2e^2/h$. Here we have taken a value of $R_{\mathrm{contact}} = h/e^2$ for illustration; other R_{contact} values can be used with no qualitative changes.

$\exp[-\tilde{\beta}]$ for $\tilde{\beta} \gg 1$. Interestingly for small T, $\mathcal{F} \to 1$, reflecting the (band) geometrical origin of anomalous transverse diffusion. We note that σ_H^v, D_H^v do not vary significantly for **E**-induced shifts in $\mu_{l\alpha} < \Delta$; sizable valley imbalances along the edge can accumulate in the linear response regime.

Writing $D_H^v = D_H^{l,(\alpha=+1)}$ [see Eq. (5)] yields the resistivity of the quasi-1D channels along the sample edges

$$\rho_{1d}(T) = \frac{\rho_0}{\tilde{\beta}^{1/2}\mathcal{F}(\tilde{\beta})}, \quad \rho_0 = \frac{2\Delta^{3/2}(\eta/e)^{1/2}}{\hbar v^2 \tau_v^{1/2}|\sigma_H^v|}, \tag{12}$$

where ρ_0 is the characteristic 1D resistivity; see also Appendix E.

The term ρ_0 is nonuniversal and depends on the rate of relaxation of different parts of the Fermi surface at K and K' encoded in the intervalley scattering time τ_v. In a bulk homogeneous sample with few short-range impurities, intervalley scattering can be long (on the order of ten to several tens of picoseconds [15–17]). Further, it has been noticed in Ref. [26] that the notion of valleys is preserved for *generic* edge terminations in graphene since generic terminations are described by zigzag-type boundary conditions. Even so, the specific edge termination configuration may enable enhanced intervalley scattering (as compared with the bulk), for example through edge roughness or via indirect scattering processes through flat or weakly dispersive edge states [27], and the value of τ_v can be accordingly reduced close to edges. For these reasons, in Fig. 2 we have chosen to illustrate SEC by presenting the values of $\rho_{1d}(T)$ associated with a range of values of $\tau_v \sim$1–10 ps. Strikingly, even for relatively fast intervalley scattering $\tau_v \sim 1$ ps, ρ_{1d} can still take on small values $\rho_{1d} \sim h/e^2$ μm^{-1}; see Fig. 2(a) (red curve). In contrast, the bulk resistance exponentially rises at low temperatures, $R_{\mathrm{bulk}} \propto \exp(\Delta/k_BT)$, where Δ is the half-gap size. As a result, for small gap sizes of tens of meV, sufficiently short lengths, and low temperatures, SEC possesses a very small resistivity [dominating R^{-1} in Eq. (10)] and can mimic a low-dissipation quasi-one-dimensional channel that shunts the bulk; see Fig. 2(b).

We note that in the low-temperature regime where $(\rho_{1d}L) \ll R_{\mathrm{contact}}$, Eq. (10) is dominated by the contact resistance; see Fig. 2(b). As a result of the low dissipation in the SEC channel, current-voltage characteristics in a two-terminal geometry may display only very weakly L-dependent characteristics.

V. DISCUSSION

It is useful to point out some of the conceptual differences between conventional bulk transport in electronic systems and SEC. Bulk carrier transport in electronic systems is typically characterized by a *homogeneous flow* of current density through the sample that is sustained by an electric field that accelerates the charge carriers. This electric field displaces the Fermi surface in momentum space so that larger current density corresponds to a larger relative displacement of the Fermi surface in momentum space. In contrast, SEC arises from an *inhomogeneous flow* of current density running along the edges of the device. For SEC, the charge carriers are not accelerated along the flow direction (**y**); instead SEC is sustained by an inhomogeneous valley density profile $n_v(x)$ in real space (along **x**) induced by an electric field (along **y**).

Crucially, larger SEC current corresponds to a larger local steady-state valley density (close to the edges in real space); see Eq. (9). Interestingly, as detailed below, even in the linear response regime, this *steady-state* out-of-equilibrium valley density can be far larger than equilibrium density of thermally activated carriers when the chemical potential is in the gap and at low temperatures. This is in stark contrast to what is expected in conventional bulk transport, where electronic density is kept uniform and close to its equilibrium value even when current is flowing through. Where does this large density of carriers come from? As we now argue, the increased local steady-state valley density can be fed by the source/drain contacts that inject carriers that are shunted along the SEC channels. This can be understood as follows. Charge transport occurs when carriers are injected from a source contact, and removed at a drain contact. After short time transients, the device reaches a steady state with the amount of current injected (at source contact) equal to the amount of current removed (at drain contact), resulting in a steady-state distribution of carriers. For our system, this steady-state out-of-equilibrium distribution of carriers is determined by Eq. (6), allowing sizable steady-state local valley densities to be accumulated along the edges.

We now estimate the maximal valley density, n_v^*, that can be accumulated along the edges [as determined by Eq. (6)] concentrating on the regime of μ in the gap and $k_BT < \Delta$. To proceed, we note that the validity of linear response theory requires that the values of D, σ_{xy}^v (as well as D_H^v when considering the SEC current; see below) used do not change much as valley density is accumulated at the edge of the sample. For gapped graphene with equilibrium chemical potential initially in the gap, this requires the electric-field-induced change in the quasi-Fermi levels (close to the edges) to satisfy $\delta\mu_{e,h}^{K,K'} \ll \Delta$. This is because the relevant transport coefficients for SEC

(D, σ^v_{xy}, and D^v_H) do not vary appreciably as chemical potential is changed inside the gap [28]; in fact, σ^v_{xy} and D^v_H both reach their maximal values inside the gap. The condition on quasi-Fermi levels can be immediately translated into one for density so that linear response is satisfied for $n_v \ll n^*_v$, where $n^*_v = \mathcal{N}\int_\Delta^\infty d\epsilon\, \nu(\epsilon)\{1+\exp[(\epsilon-\Delta)/k_BT]\}^{-1}$, where $\nu(\epsilon)$ is the density of states, and $\mathcal{N}$ is the valley/flavor and spin degeneracy. Using the density of states of a gapped Dirac cone, we obtain

$$n^*_v = \mathcal{N}[12\ln(2)k_BT\Delta + \pi^2(k_BT)^2]/(24\pi v^2\hbar^2). \tag{13}$$

Unusually, $n^*_v \propto T$ can be much larger than the thermally activated carrier density at equilibrium [$n^{\rm eq}_T \propto \exp(-\Delta/k_BT)$]. As discussed above, this *steady-state* n_v builds up and is fed by the source/drain contacts that inject/remove a steady flow of carriers.

A related quantity is the critical SEC, I^*, that can be carried by the system through the SEC channels along the edges ($I_{\rm SEC} \ll I^*$) in order to remain in the linear response regime. The term $\mathbf{j}^{\rm SEC}_c$ is directly proportional to the amplitude of $n_v(x)$, see Eq. (9), and integrating over the SEC channel width we obtain the critical SEC current as

$$I^* = eD^v_H n^*_v \approx \frac{e\mathcal{N}}{2h}k_BT\ln 2 + O(T^2/\Delta), \tag{14}$$

where we have used the value of D^v_H in Eq. (11) for small T, substituted Eq. (13), and kept the leading terms in T. Taking $\mathcal{N}=4$ and taking $k_BT = 1$ meV, we obtain sizable $I^*{\sim}0.053\ \mu$A, allowing significant SEC to be run through the device with low dissipation. Interestingly, we note that I^* vanishes as $T\to 0$, indicating that while SEC resistivity slowly decreases as T decreases, the amount of current these channels can sustain (in the linear response regime) also vanishes.

The nonactivated conductance, as well as nonactivated valley density, sustained at the edges of the sample of SEC is distinct from that of conventional transport. Indeed, the fact that valley densities n^*_v that can be sustained are far larger than the thermally activated density at equilibrium $n^{\rm eq}_T$ suggests that SEC is an out-of-*local*-equilibrium effect; nevertheless it can still possess linear response characteristics, as detailed above.

SEC here replicates the unusual transport characteristics found in recent gapped graphene-type structures (G/hBN and gapped bilayer graphene devices) [18]. For example, Fig. 1 mirrors the sharp spatial edge current distribution in gapped graphene-type structures found in Ref. [18] using Josephson current spectroscopy. Further, a saturation of device resistance (up to a few resistance quanta) was measured in Hall bars even at low temperatures (∼10 K), while Corbino geometry measurements of the same samples showed fully activated behavior; this directly reproduces SEC characteristics in Fig. 2(b). Further, we note that recent Kerr-rotation microscopy in biased monolayer MoS_2 shows magnetization accumulated along edges [13,14], another signature of valley imbalance accumulation and SEC along the edge. We emphasize that while neither gapped graphene (G/hBN or gapped bilayer graphene) nor MoS_2 possess topological gapless edge states, they possess strong Berry curvature close to their band edges, enabling the unusual quantum-geometry-mediated transport (such as SEC) in these systems [13,14,18].

Bloch-band quantum geometry can play a crucial role in charge transport of time-reversal-invariant materials as epitomized by SEC that mimic ballistic edge channels without (spectral) edge states. SEC exhibits striking nonactivated behavior even in nominally bulk insulating and topologically trivial devices. Additionally, SEC also mediates spin-free magnetoelectric coupling, an unusual characteristic of these "trivial" insulators with nonvanishing Berry curvature; band geometry naturally interlaces charge and magnetization degrees of freedom even in a spin-orbit-free system.

ACKNOWLEDGMENTS

We gratefully acknowledge useful conversations with Dima Pesin, Mark Runder, Maksym Serbyn, and Valla Fatemi. J.C.W.S. acknowledges support from the Singapore National Research Foundation (NRF) under NRF Fellowship Award No. NRF-NRFF2016-05, as well as Nanyang Technological University Singapore through a start-up grant. G.V. acknowledges generous support from the CA2DM, where this work was initiated, and from NSF Grant No. DMR-1406568.

APPENDIX A: COVARIANT DERIVATIVE AND ANOMALOUS VELOCITY

As a warm-up, we briefly review the covariant derivative. Our starting point is the gauge-invariant (physical) position operator in the Bloch representation

$$\hat{\mathbf{r}}_{l\alpha} = i\frac{\partial}{\partial\mathbf{k}} + \boldsymbol{\mathcal{A}}_{l\alpha}(\mathbf{k}), \tag{A1}$$

where $\boldsymbol{\mathcal{A}}_{l\alpha}(\mathbf{k}) = i\langle u_{l\alpha}(\mathbf{k})|\partial_{\mathbf{k}}u_{l\alpha}(\mathbf{k})\rangle$ is the Berry connection of the band and valley under consideration. We note that $i\frac{\partial}{\partial\mathbf{k}}$ is the canonical (non-gauge-invariant) position operator in the momentum representation. Crucially, different components of $\hat{\mathbf{r}}$ do not commute with each other. In particular,

$$[\hat{r}_i, \hat{r}_j] = i\big(\partial_{k_i}[\mathcal{A}_{l\alpha}]_j - \partial_{k_j}[\mathcal{A}_{l\alpha}]_i\big) \equiv i\varepsilon_{ijk}\Omega_k, \tag{A2}$$

where the Berry curvature is

$$\Omega_i \equiv \varepsilon_{ijk}\partial_{k_j}[\mathcal{A}_{l\alpha}]_k. \tag{A3}$$

In the presence of an applied electric field, the Hamiltonian reads as $\hat{H} = \epsilon_n(\mathbf{k}) - (-e)\mathbf{E}\cdot\hat{\mathbf{r}}$. Here $-e<0$ is the electron charge, and $\mathbf{E}$ is the electric field. Writing the velocity as $\hat{\mathbf{v}} = \frac{1}{i\hbar}[\hat{\mathbf{r}}, \hat{H}]$, we obtain

$$\langle\hat{v}_i\rangle = \frac{1}{i\hbar}\langle[r_i, \hat{H}]\rangle = \frac{1}{\hbar}\frac{\partial\epsilon_n(\mathbf{k})}{\partial_{k_i}} - \frac{ie}{\hbar}\langle[\hat{r}_i, \hat{r}_j]\rangle E_j \tag{A4}$$

$$= \frac{1}{\hbar}\frac{\partial\epsilon_n(\mathbf{k})}{\partial k_i} + \frac{e}{\hbar}\varepsilon_{ijk}E_j\Omega_k, \tag{A5}$$

where the second term is the anomalous velocity.

APPENDIX B: MAGNETIC MOMENT AND INHOMOGENEOUS CURRENT DENSITY

In this Appendix, we discuss the relationship between the magnetic moment and the inhomogeneous current density in Eq. (2) of the main text.

We begin by noting that the magnetic moment

$$\hat{\mathbf{m}} = -\frac{e}{4}(\hat{\mathbf{r}} \times \hat{\mathbf{v}} - \hat{\mathbf{v}} \times \hat{\mathbf{r}}) = \frac{ie}{4\hbar}(\hat{\mathbf{r}} \times [\hat{\mathbf{r}}, \hat{H}] - [\hat{\mathbf{r}}, \hat{H}] \times \hat{\mathbf{r}}), \tag{B1}$$

where $\hat{H}$ is the Hamiltonian and $\hat{\mathbf{v}} = -i\hbar^{-1}[\hat{\mathbf{r}}, \hat{H}]$. It is important to notice that at this stage the operator $\hat{\mathbf{r}}$ is not yet projected on a given band. Thus, interband matrix elements of $\hat{\mathbf{r}}$ are still included. However, the Hamiltonian is diagonal in the band representation. The magnetic moment can be reexpressed in component form as

$$m_i = \frac{ie}{4\hbar}\varepsilon_{ijk}(\hat{r}_j\hat{r}_k\hat{H} - \hat{r}_j\hat{H}\hat{r}_k - \hat{r}_j\hat{H}\hat{r}_k + \hat{H}\hat{r}_j\hat{r}_k), \tag{B2}$$

where a sum over repeated indices is implied. This can be recast as

$$i\varepsilon_{ijk}q_jm_k = \frac{e}{2\hbar}q_j[\hat{r}_i\hat{H}\hat{r}_j - \hat{r}_j\hat{H}\hat{r}_i] - \frac{e}{2\hbar}q_j\left[\frac{\hat{H}(\hat{r}_i\hat{r}_j - \hat{r}_j\hat{r}_i)}{2} + \frac{(\hat{r}_i\hat{r}_j - \hat{r}_j\hat{r}_i)\hat{H}}{2}\right]. \tag{B3}$$

Now we make use of the commutation relation

$$\hat{\mathbf{r}} \times \hat{\mathbf{r}} = i\hat{\mathbf{\Omega}}, \tag{B4}$$

where $\hat{\mathbf{\Omega}}$ is the Berry curvature *operator* defined as the covariant derivative of the Berry connection in the full Hilbert space, to rewrite m_i as

$$m_i = -\frac{ie}{2\hbar}\varepsilon_{ijk}\hat{r}_j\hat{H}\hat{r}_k - \frac{e}{4\hbar}[\hat{\Omega}_i\hat{H} + \hat{H}\hat{\Omega}_i]. \tag{B5}$$

We can now take the diagonal matrix element of this operator in the band of interest, say $l\alpha$, and noting that $\hat{\mathbf{r}} = i\nabla_{\mathbf{k}}$, where $\nabla_{\mathbf{k}} = \partial_{\mathbf{k}} - i\mathcal{A}(\mathbf{k})$ is the covariant derivative (still an operator in the full Hilbert space), and that the diagonal matrix element of $\hat{\mathbf{\Omega}}$ is

$$\Omega_{l\alpha}(\mathbf{k}) = i\langle\nabla_{\mathbf{k}}u_{l\alpha}(\mathbf{k})| \times |\nabla_{\mathbf{k}}u_{l\alpha}(\mathbf{k})\rangle, \tag{B6}$$

we recover the well-known formula [19,20]

$$\mathbf{m}_{l\alpha}(\mathbf{k}) = \frac{ie}{2\hbar}\langle\nabla_{\mathbf{k}}u_{l\alpha}(\mathbf{k})|[\epsilon_{l\alpha}(\mathbf{k}) - \hat{H}] \times |\nabla_{\mathbf{k}}u_{l\alpha}(\mathbf{k})\rangle. \tag{B7}$$

Similarly, we write the q-linear part of the current density operator in Eq. (2) of the main text (denoted by $\hat{\mathbf{j}}^{(1)}_{\mathbf{q},i}$) in component form as

$$\hat{j}^{(1)}_{\mathbf{q},i} = i\frac{e}{2}q_i(\hat{v}_j\hat{r}_i + \hat{r}_i\hat{v}_j) = \frac{e}{2\hbar}q_i(\hat{r}_j\hat{H}\hat{r}_i - \hat{H}\hat{r}_j\hat{r}_i + \hat{r}_i\hat{r}_j\hat{H} - \hat{r}_i\hat{H}\hat{r}_j). \tag{B8}$$

After some algebra, this can be recast in the following form:

$$\hat{j}^{(1)}_{\mathbf{q},i} = \frac{e}{2\hbar}q_j[\hat{r}_i\hat{H}\hat{r}_j - \hat{r}_j\hat{H}\hat{r}_i] - \frac{e}{2\hbar}q_j\left[\frac{\hat{H}(\hat{r}_i\hat{r}_j - \hat{r}_j\hat{r}_i)}{2} + \frac{(\hat{r}_i\hat{r}_j - \hat{r}_j\hat{r}_i)\hat{H}}{2}\right] + \frac{e}{2\hbar}q_i\left[\hat{H}\frac{\hat{r}_i\hat{r}_j + \hat{r}_j\hat{r}_i}{2} - \frac{\hat{r}_i\hat{r}_j + \hat{r}_j\hat{r}_i}{2}\hat{H}\right]. \tag{B9}$$

The first two lines of this equation reproduce Eq. (B3) exactly. The last line is, in general, nonzero, but vanishes when averaged in a single band because the $\hat{H}$ operators become numbers $\hat{H} \to \epsilon_{l\alpha}(\mathbf{k})$, and what remains is the difference of two identical terms. We conclude that

$$\left[\hat{j}^{(1)}_{\mathbf{q},i}\right]_{l\alpha} = i\varepsilon_{ijk}q_jm_{l\alpha,k} \tag{B10}$$

or, in real space,

$$[\hat{\mathbf{j}}^{(1)}(\mathbf{r})]_{l\alpha} = \nabla_{\mathbf{r}} \times \mathbf{m}_{l\alpha}(\mathbf{r}). \tag{B11}$$

Taking $\mathbf{m}_{l\alpha}(\mathbf{r}) = \sum_{\mathbf{k}} f_{l\alpha}(\mathbf{k}, \mathbf{r})\mathbf{m}_{l\alpha}(\mathbf{k})$ we recover Eq. (3) of the main text.

APPENDIX C: MAGNETIC MOMENT FOR GAPPED GRAPHENE

Here we briefly derive (for the convenience of the reader) the well-known relation between Berry curvature and the magnetic moment for gapped graphene, namely,

$$\mathbf{m}_{\ell\alpha}(\mathbf{k}) = \frac{e}{\hbar}\epsilon_{\mathbf{k},\ell}\mathbf{\Omega}_{\ell\alpha}(\mathbf{k}). \tag{C1}$$

Equation (C1) can be shown in a straightforward fashion by recalling that the magnetic moment is

$$\langle\hat{\mathbf{M}}\rangle_{\ell,\alpha} = \frac{ie}{2\hbar}\langle\nabla_{\mathbf{k}}u_{\ell\alpha}(\mathbf{k})|e[\epsilon_\ell(\mathbf{k}) - \hat{H}] \times |\nabla_{\mathbf{k}}u_{\ell\alpha}(\mathbf{k})\rangle. \tag{C2}$$

Noting that for the two-band, particle-hole symmetric system $\epsilon_{\ell=+}(\mathbf{k}) = -\epsilon_{\ell=-}(\mathbf{k})$, we have

$$\epsilon_\ell(\mathbf{k}) - \hat{H}_\alpha = 2\epsilon_\ell(\mathbf{k})|u_{n\neq\ell,\alpha}(\mathbf{k})\rangle\langle u_{n\neq\ell,\alpha}(\mathbf{k})|. \tag{C3}$$

Inserting into Eq. (C2) we obtain

$$\langle\hat{\mathbf{M}}\rangle_{\ell,\alpha} = \frac{ie\epsilon_\ell}{\hbar}\left[\left\langle\frac{\partial u_{\ell,\alpha}}{\partial k_x}\middle|\frac{\partial u_{\ell,\alpha}}{\partial k_y}\right\rangle - \left\langle\frac{\partial u_{\ell,\alpha}}{\partial k_y}\middle|\frac{\partial u_{\ell,\alpha}}{\partial k_x}\right\rangle\right], \tag{C4}$$

where we have applied the resolution of the identity. Recalling that the Berry curvature is simply $\mathbf{\Omega}_{\ell\alpha}(\mathbf{k}) = i\langle\nabla_{\mathbf{k}}u_{\ell\alpha}(\mathbf{k})| \times |\nabla_{\mathbf{k}}u_{\ell\alpha}(\mathbf{k})\rangle$, we obtain Eq. (C1).

APPENDIX D: ALTERNATIVE DERIVATION OF INHOMOGENEOUS CURRENT DENSITY: VELOCITY MATRIX ELEMENT

In this section, we discuss an alternative algebraic derivation of the inhomogeneous current density by expanding the velocity matrix element at finite $\mathbf{q}$. For brevity, we will suppress the flavor index α leaving only the band index l without loss of any generality. While less compact than the above discussion (using the magnetic moment operator), this alternative approach explicitly shows how the accumulation of geometric phases at finite $\mathbf{q}$ leads to the anomalous transverse diffusion.

We proceed by considering the current dynamics in Bloch bands with a spatially varying out-of-equilibrium carrier density in the absence of an applied magnetic field. The current density $\mathbf{j}_l(\mathbf{r}) = e\sum_{\mathbf{q}}\mathbf{v}^{(l)}_{\mathbf{q}}e^{i\mathbf{q}\cdot\mathbf{r}}$ can be expressed in terms of its Fourier harmonics as

$$\mathbf{v}^{(l)}_{\mathbf{q}} = \sum_{\mathbf{k}} c^\dagger_{\mathbf{k}_-,l}\langle l, \mathbf{k}_-|\hat{\mathbf{v}}|l, \mathbf{k}_+\rangle c_{\mathbf{k}_+,l}, \quad \hbar\hat{\mathbf{v}} = \frac{\partial\hat{H}}{\partial\mathbf{k}}, \tag{D1}$$

where $\hat{\mathbf{v}}$ is the velocity operator, $\hat{H}$ is the Hamiltonian, $\mathbf{k}_\pm = \mathbf{k} + \mathbf{q}/2$, and $c^\dagger_{\mathbf{k},l}$ is a creation operator for quasiparticles in band l with corresponding (Bloch) wave function $\langle \mathbf{r}|c^\dagger_{\mathbf{k},l}|0\rangle = \langle \mathbf{r}|l,\mathbf{k}\rangle e^{i\mathbf{k}\cdot\mathbf{r}}$. The crystal wave functions $\langle \mathbf{r}|n,\mathbf{k}\rangle = u_{l,\mathbf{k}}(\mathbf{r})$ are periodic over the unit cell.

As we now demonstrate, the phases accumulated by quasiparticles in the bands can play a crucial role in their transport, producing anomalous current flow when the carrier density is inhomogeneous. To illustrate this, we first note that the wave function $\langle \mathbf{r}|l,\mathbf{k}+\mathbf{q}\rangle$ can be expanded, to leading order in $\mathbf{q}$, as

$$\langle \mathbf{r}|l,\mathbf{k}\rangle + \left(\left\langle \mathbf{r}\middle|\frac{\partial u_{l,\mathbf{k}}}{\partial \mathbf{k}_i}\right\rangle - i\mathcal{A}_{l,i}(\mathbf{k})\left\langle \mathbf{r}\middle|u_{l,\mathbf{k}}\right\rangle\right)\mathbf{q}_i + \cdots, \quad \text{(D2)}$$

where we have expressed the expansion in component form, and $\mathcal{A}_{l,i}(\mathbf{k}) = \boldsymbol{\mathcal{A}}_l(\mathbf{k})\cdot\hat{\mathbf{x}}_i$ is the ith component of the Berry connection $\boldsymbol{\mathcal{A}}_l(\mathbf{k}) = i\langle u_{l,\mathbf{k}}|\partial_{\mathbf{k}}|u_{l,\mathbf{k}}\rangle$ (i.e., $\boldsymbol{\mathcal{A}}_l$ in the $\hat{\mathbf{x}}_i$ direction). Notice that the Taylor expansion in $\mathbf{k}$ is done using the covariant derivative, $\boldsymbol{\nabla}_{\mathbf{k}} = \partial_{\mathbf{k}} - i\boldsymbol{\mathcal{A}}_l(\mathbf{k})$; this is needed to ensure that the calculated current is physical, i.e., invariant under a "gauge transformation" of the crystal wave function, $u_{l,\mathbf{k}}(\mathbf{r}) \to e^{-i\chi(\mathbf{k})}u_{l,\mathbf{k}}(\mathbf{r})$.

Applying the expansion of the wave function at small $\mathbf{q}$ described in Eq. (D2) to the velocity matrix element, we obtain

$$\langle l,\mathbf{k}_-|\hat{\mathbf{v}}_i|l,\mathbf{k}_+\rangle = \langle l,\mathbf{k}|\hat{\mathbf{v}}_i|l,\mathbf{k}\rangle + \left[\mathcal{C}^{(l)}_{ij}(\mathbf{k})\right](i\mathbf{q}_j) + O(q^2), \quad \text{(D3)}$$

where $\hbar\langle l,\mathbf{k}|\hat{\mathbf{v}}_i|l,\mathbf{k}\rangle = \frac{\partial\epsilon_l(\mathbf{k})}{\partial\mathbf{k}_i}$ is the group velocity, and

$$\begin{aligned}\left[\mathcal{C}^{(l)}_{ij}(\mathbf{k})\right](i\mathbf{q}_j) &= \left[\left\langle\frac{\partial u_{l,\mathbf{k}}}{\partial\mathbf{k}_j}\middle|\hat{\mathbf{v}}_i|u_{l,\mathbf{k}}\right\rangle - \langle u_{l,\mathbf{k}}|\hat{\mathbf{v}}_i\left|\frac{\partial u_{l,\mathbf{k}}}{\partial\mathbf{k}_j}\right\rangle\right]\frac{\mathbf{q}_j}{2} \\ &\quad - 2i\langle u_{l,\mathbf{k}}|\hat{\mathbf{v}}_i|u_{l,\mathbf{k}}\rangle\mathcal{A}_j\frac{\mathbf{q}_j}{2} \\ &= \sum_m\left[\left\langle\frac{\partial u_{l,\mathbf{k}}}{\partial\mathbf{k}_j}\middle|u_{m,\mathbf{k}}\right\rangle\langle u_{m,\mathbf{k}}|\hat{\mathbf{v}}_i|u_{l,\mathbf{k}}\rangle\right. \\ &\quad \left. - \langle u_{l,\mathbf{k}}|\hat{\mathbf{v}}_i|u_{m,\mathbf{k}}\rangle\left\langle u_{m,\mathbf{k}}\middle|\frac{\partial u_{l,\mathbf{k}}}{\partial\mathbf{k}_j}\right\rangle\right]\frac{\mathbf{q}_j}{2} \\ &\quad - 2i\langle u_{l,\mathbf{k}}|\hat{\mathbf{v}}_i|u_{l,\mathbf{k}}\rangle\mathcal{A}_j\frac{\mathbf{q}_j}{2}. \end{aligned} \quad \text{(D4)}$$

In the last line we have inserted the resolution of the identity $\sum_m |u_{m,\mathbf{k}}\rangle\langle u_{m,\mathbf{k}}| = 1$ into the terms of the square parentheses.

In order to proceed, we note that when $m = l$, the square parentheses cancel with the last term since $\langle u_{l,\mathbf{k}}|\frac{\partial u_{l,\mathbf{k}}}{\partial\mathbf{k}_j}\rangle = -i\mathcal{A}_j$. As a result, only terms with $m \neq l$ remain in Eq. (D4). Using the identity for the interband matrix element

$$\hbar\langle u_{l,\mathbf{k}}|\hat{\mathbf{v}}_i|u_{m,\mathbf{k}}\rangle = \left\langle u_{l,\mathbf{k}}\middle|\frac{\partial u_{m,\mathbf{k}}}{\partial k_i}\right\rangle[\epsilon_l(\mathbf{k}) - \epsilon_m(\mathbf{k})], \quad l \neq m, \quad \text{(D5)}$$

where $\epsilon_l(\mathbf{k})$ is the quasiparticle energy in band l, yields

$$\mathcal{C}^{(l)}_{ij} = -\frac{i}{2\hbar}\sum_{m\neq l}\left\langle\frac{\partial u_{l,\mathbf{k}}}{\partial k_i}\middle|u_{m,\mathbf{k}}\right\rangle[\epsilon_l(\mathbf{k}) - \epsilon_m(\mathbf{k})]\left\langle u_{m,\mathbf{k}}\middle|\frac{\partial u_{l,\mathbf{k}}}{\partial k_j}\right\rangle - \text{c.c.} \quad \text{(D6)}$$

Comparing this with the well-known expression for the magnetic moment [19,20]

$$\langle\hat{\mathbf{M}}\rangle = \frac{ie}{2\hbar}\langle\boldsymbol{\nabla}_{\mathbf{k}}u_{l\alpha}(\mathbf{k})|[\epsilon_{l\alpha}(\mathbf{k}) - \hat{H}]\times|\boldsymbol{\nabla}_{\mathbf{k}}u_{l\alpha}(\mathbf{k})\rangle \quad \text{(D7)}$$

yields Eq. (3) of the main text.

APPENDIX E: ESTIMATE OF CHARACTERISTIC SEC RESISTIVITY

In the following we give a simple estimate of the characteristic SEC resistivity. Recalling Eq. (12) of the main text, we have the resistivity of the SEC channel

$$\rho_{1\mathrm{d}}(T) = \frac{\rho_0}{\tilde{\beta}^{1/2}\mathcal{F}(\tilde{\beta})}, \quad \rho_0 = \frac{2\Delta^{3/2}(\eta/e)^{1/2}}{\hbar v^2\tau_v^{1/2}|\sigma_H^v|}, \quad \text{(E1)}$$

where ρ_0 is the characteristic 1D resistivity and can be estimated as

$$\rho_0 = 0.48\frac{(\Delta[\mathrm{meV}]/10)^{3/2}\{\eta[\mathrm{m}^2/(\mathrm{V\ s})]\}^{1/2}}{(\tau_v[\mathrm{ps}]/10)^{1/2}}\left[\frac{h}{e^2}\ \mu\mathrm{m}^{-1}\right], \quad \text{(E2)}$$

where we have used $v = 10^6$ m/s, and taken $|\sigma_H^v| = 2e^2/h$.

We note that for narrow-gapped Dirac materials $\Delta\sim$10 meV, ρ_0 can be as small as fractions of the quantum of resistance h/e^2. As a result, at low temperatures, $\rho_{1\mathrm{d}}(T)$ in Eq. (E1) yields low-dissipation squeezed edge channels. When the value of ρ_0 in Eq. (E1) for such narrow-gapped Dirac materials is substituted into Eq. (10), we find the low-dissipation $\rho_{1d}L$ can become far smaller than R_{contact}. As a result, R_{SEC} [red line in Fig. 2(b)] becomes dominated by R_{contact} and tends to the R_{contact} [dashed line in Fig. 2(b)] value at low temperature.

As discussed in the main text, this behavior was recently seen in gapped graphene-type structures [18], where a saturation of device resistance (up to a few resistance quanta) was measured in Hall bars even at low temperatures ($\sim$10 K; where SEC is operative), while Corbino geometry measurements (where edge contributions are eliminated) of the same samples showed fully activated behavior.

In contrast, for large gapped Dirac materials $\Delta\sim$1 eV, ρ_0 can be many times larger; for example, taking $\Delta = 1$ eV, $\eta = 1$ m^2/(V s), and $\tau_v = 1$ ps, we obtain a very resistive channel $\rho_0\approx$40 MΩ μm^{-1}. These values are so large as to be comparable with the bulk resistance, making SEC an ineffective current shunt to bulk charge current conduction.

As a result, we conclude that narrow-gapped Dirac materials (e.g., G/hBN or gapped bilayer graphene) at low temperature are ideal platforms to observe low-dissipation squeezed edge currents (as seen in Fig. 2 of the main text; compare also with Hall bar device resistances observed in Ref. [18]).

[1] N. W. Ashcroft and N. D. Mermin, *Solid State Physics* (Brooks/Cole Cengage Learning, 1976).

[2] D. J. Thouless, M. Kohmoto, M. P. Nightingale, and M. den Nijs, Quantized Hall Conductance in a

Two-Dimensional Periodic Potential, Phys. Rev. Lett. **49**, 405 (1982).

[3] X. G. Wen, *Quantum Field Theory of Many-Body Systems: From the Origin of Sound to an Origin of Light and Electrons* (Oxford University Press, 2004).

[4] B. I. Halperin, Quantized Hall conductance, current-carrying edge states, and the existence of extended states in a two-dimensional disordered potential, Phys. Rev. B **25**, 2185 (1982).

[5] M. Büttiker, Absence of backscattering in the quantum Hall effect in multiprobe conductors, Phys. Rev. B **38**, 9375 (1988).

[6] M. Z. Hasan and C. L. Kane, *Colloquium:* Topological insulators, Rev. Mod. Phys. **82**, 3045 (2010).

[7] Y. Hatsugai, Chern Number and Edge States in the Integer Quantum Hall Effect, Phys. Rev. Lett. **71**, 3697 (1993).

[8] A. H. MacDonald and P. Středa, Quantized Hall effect and edge currents, Phys. Rev. B **29**, 1616 (1984).

[9] D. Xiao, W. Yao, and Q. Niu, Valley-Contrasting Physics in Graphene: Magnetic Moment and Topological Transport, Phys. Rev. Lett. **99**, 236809 (2007).

[10] N. Fabrizio, H. J. Suominen, M. Kjaergaard, C. M. Marcus, E. Sajadi, J. A. Folk, F. Qu, A. J. A. Beukman, F. K. de Vries, J. van Veen, S. Nadj-Perge, L. P. Kouwenhoven, B.-M. Nguyen, A. A. Kiselev, W. Yi, M. Sokolich, M. J. Manfra, E. M. Spanton, and K. A. Moler, Edge transport in the trivial phase of InAs/GaSb, New J. Phys. **18**, 083005 (2016).

[11] A. J. A. Beukman, Topology in two-dimensional systems, Ph.D. thesis, TU Delft, Sec. 7.3, 2016.

[12] J. Li, I. Martin, M. Büttiker, and A. F. Morpurgo, Topological origin of subgap conductance in insulating bilayer graphene, Nat. Phys. **7**, 38 (2011).

[13] J. Lee, K. F. Mak, and J. Shan, Electrical control of the valley Hall effect in bilayer MoS_2 transistors, Nat. Nanotechnol. **11**, 421 (2016).

[14] J. Lee, Z. Wang, H. Xie, K. F. Mak, and J. Shan, Valley magnetoelectricity in single-layer MoS_2, Nat. Mater. **16**, 887 (2017).

[15] R. V. Gorbachev, J. C. W. Song, G. L. Yu, A. V. Kretinin, F. Withers, Y. Cao, A. Mishchenko, I. V. Grigorieva, K. S. Novoselov, L. S. Levitov, and A. K. Geim, Detecting topological currents in graphene superlattices, Science **346**, 448 (2014).

[16] Y. Shimazaki, M. Yamamoto, I. V. Borzenets, K. Watanabe, T. Taniguchi, and S. Tarucha, Generation and detection of pure valley current by electrically induced Berry curvature in bilayer graphene, Nat. Phys. **11**, 1032 (2015).

[17] M. Sui, G. Chen, L. Ma, W. Shan, D. Tian, K. Watanabe, T. Taniguchi, X. Jin, W. Yao, D. Xiao, and Y. Zhang, Gate-tunable topological valley transport in bilayer graphene, Nat. Phys. **11**, 1027 (2015).

[18] M. J. Zhu, A. V. Kretinin, M. D. Thompson, D. A. Bandurin, S. Hu, G. L. Yu, J. Birkbeck, A. Mishchenko, I. J. Vera-Marun, K. Watanabe, T. Taniguchi, M. Polini, J. R. Prance, K. S. Novoselov, A. K. Geim, and M. Ben Shalom, Edge currents shunt the insulating bulk in gapped graphene, Nat. Commun. **8**, 14552 (2017).

[19] J. Shi, G. Vignale, D. Xiao, and Q. Niu, Quantum Theory of Orbital Magnetization and Its Generalization to Interacting Systems, Phys. Rev. Lett. **99**, 197202 (2007).

[20] D. Xiao, M.-C. Chang, and Q. Niu, Berry phase effects on electronic properties, Rev. Mod. Phys. **82**, 1959 (2010).

[21] D. Xiao, Y. Yao, Z. Fang, and Q. Niu, Berry-Phase Effect in Anomalous Thermoelectric Transport, Phys. Rev. Lett. **97**, 026603 (2006).

[22] D. T. Son and N. Yamamoto, Berry Curvature, Triangle Anomalies, and the Chiral Magnetic Effect in Fermi Liquids, Phys. Rev. Lett. **109**, 181602 (2012).

[23] J. P. Tetienne, N. Dontschuk, D. A. Broadway, A. Stacey, D. A. Simpson, and L. C. Hollenberg, Quantum imaging of current flow in graphene, Sci. Adv. **3**, e1602429 (2017).

[24] N. R. Cooper, B. I. Halperin, and I. M. Ruzin, Thermoelectric response of an interacting two-dimensional electron gas in a quantizing magnetic field, Phys. Rev. B **55**, 2344 (1997).

[25] Y. D. Lensky, J. C. W. Song, P. Samutpraphoot, and L. S. Levitov, Topological Valley Currents in Gapped Dirac Materials, Phys. Rev. Lett. **114**, 256601 (2015).

[26] A. R. Akhmerov and C. W. J. Beenakker, Boundary conditions for Dirac fermions on a terminated honeycomb lattice, Phys. Rev. B **77**, 085423 (2008).

[27] J. Li, A. F. Morpurgo, M. Büttiker, and I. Martin, Marginality of bulk-edge correspondence for single-valley Hamiltonians, Phys. Rev. B **82**, 245404 (2010).

[28] This behavior is in juxtaposition to that expected of the bulk longitudinal conductivity, which is exponentially sensitive to small changes in (quasi)chemical potential in the gap.